Supplementary Material

Colloidal mobilization of arsenic from mining-affected soils by surface runoff

Miguel Angel Gomez-Gonzalez [a], Andreas Voegelin [b], Javier Garcia-Guinea [a], Eduardo Bolea [c], Francisco Laborda [c], Fernando Garrido [a]

[a] *Museo Nacional de Ciencias Naturales (MNCN, CSIC). C/ Jose Gutierrez Abascal 2, 28006, Madrid, Spain*

[b] *EAWAG, Swiss Federal Institute of Aquatic Science and Technology. Ueberlandstrasse 133, 8600 Duebendorf, Switzerland*

[c] *Instituto Universitario de Ciencias Ambientales (IUCA), Universidad de Zaragoza. C/ Pedro Cerbuna 12, 50009, Zaragoza, Spain*

(5 Tables, 8 Figures)

Table of Contents

S1. Experimental locations and characterization procedures

Rainfall simulations tests were performed at the following locations: A) the arsenic-bearing waste pile (WP); B) the river bed (RB) of a small stream (~ 1 m wide) that seasonally collects surface runoff from WP; and C) the sediment that accumulates downstream in an artificial sedimentation pond (SP) (Figure S1) (Recio-Vazquez et al., 2011).

Bulk soils form WP, RB and SP were characterized as follows: Texture was determined by the pipette method after removing soil organic matter (Gee and Bauder, 1986). Soil pH and electrical conductivity (EC) were measured in deionized water (1:5 m/m suspensions), using a Thermo Orion model 920 A^+ pH meter and a Thermo Orion model 125 A conductivity meter, respectively. Total organic carbon (TOC) was determined by wet digestion (Walkley and Black, 1934). Exchangeable bases (Ca, Mg, Na, and K) (Shuman, 1985) were extracted with 1 M NH_4OAc at pH 7 (Thomas, 1982), and exchangeable Al was extracted with 1 M KCl (Barnishel and Bertsch, 1982). Semi-quantitative mineralogical composition of the total (≤ 2 mm) fraction of the WP bulk sample was previously identified by powder X-ray diffraction (XRD) with a Philips PW-1710/00 diffractometer using the CuKα radiation with a Ni filter and a setting of 40 kV and 40 mA. Samples were carefully milled over a period of 15 min and pressed to produce pellets of powdered aliquots. XRD analyses were performed using XPOWDER software. Patterns were obtained by step scanning, from 3º to 65º 2θ, with a count for 0.5 s/step exploration speed of 7º/min and 40 kV and 40 mA in the X-ray tube. The qualitative search-matching procedure was based on the ICDDPDF2 and the DIFDATA databases. Those results are presented in Table 1.

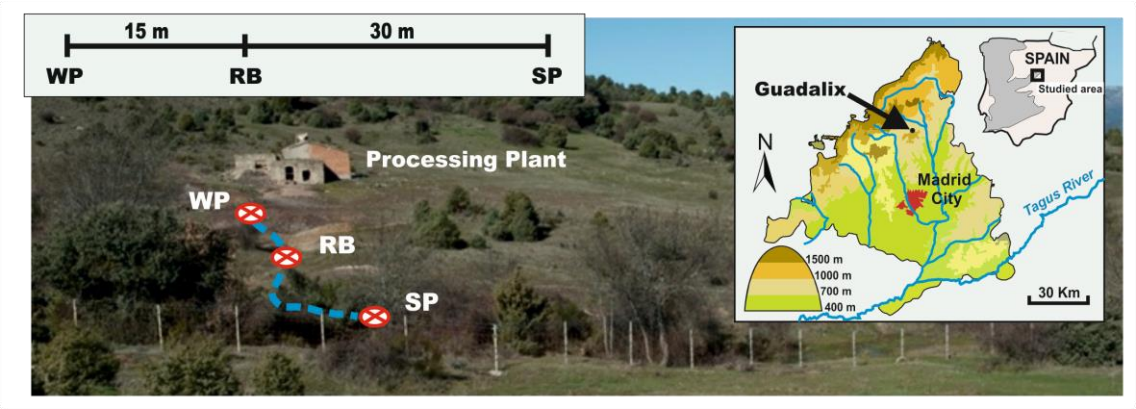

Figure S1 – Location of the studied area and relative positions of the experimental zones: Waste-pile (WP), river-bed (RB) and sedimentation-pond (SP)

S2. Rainfall simulation

S2.1. Rainfall simulator design

The sprinkling-type portable rainfall simulator to use in rugged terrain conditions and has been used for decades in a semi-arid environments with good results. The rainfall simulator is an improvement of the design of Calvo et al. (1988), modified and optimized by Cerda et al. (1997). The drop distribution generated by this rainfall simulation presents a drop-size between 2.49-2.53 mm of diameter. In all cases, the height of the outlet nozzle was set at 175 cm from the soil surface generating a drop velocity of 3.1 $m \cdot s^{-1}$ and a mean drop-size equal to 2.5 mm in diameter as tabulated by Cerda et al. (1997). The basic components of the rainfall simulator are shown in Figure S2 and described as follows:

- Upper structure and nozzle: The structure consists of a square platform of 40x40 cm. A cylindrical pipe which crossed the square structure presents a nozzle in the middle. The nozzle is a HARDI-1553-10, and has installed a filter with a mesh of 0.3 mm, a piece to increase the size of the drops and a diffuser. Four telescopic connections of 3.45 m long are connected with the square structure.

- Pumping system: The water was supplied manually for giving a better stability to the water pressure. The low water flow required (28 mm h^{-1}) allow to use hand air-compressed pumps (Matabi, Kima 12). Distilled water was used to perform the rainfall simulation processes.
- Wind protector: An important part of the rainfall simulator is the wind protector, which is fitted to the upper square structure. This protection prevents possible evaporation of the smaller drops and the disturbances caused by the wind.
- Sampling plot: The rainfall area generated by the nozzle is slightly larger than 1 m^2. In order to avoid border interference, a 0.24 m^2 experimental plot made of galvanized iron (0.55 m of diameter) was used for the measurements.

Figure S2 – Rainfall simulator description: View of the rainfall simulation with the pumping system and the wind protector (a), upper structure and nozzle (b), and experimental plot (c).

S2.2. Rainfall conditions

Distilled water was used for the rainfall simulation experiments. Homogeneous rainfall distribution was achieved at a water pressure of 1.5 kg cm^{-2} (Cerda et al., 1997) and a rain intensity of 28 mm h^{-1}. The telescopic legs were height adjusted to overcome slopes of 7%, 5% and 2% at the waste-pile, river-bed and sediment-pond sampling locations, respectively. In all cases, the height of the outlet nozzle was set at 175 cm from the soil surface (Figure S3).

Rainfall simulation experiments were carried out during 60 minutes to assure a well representative storm event in agreement with the typical rainfall in the area (according to AEMET data). Runoff suspensions were continuously collected in 5-min integration intervals in the river-bed and sedimentation pond, and in 10-min integration intervals on the waste pile using acid-cleaned polypropylene bottles of 0.5 L of volume. The samples were stored at 4°C until further analyses. The rainfall simulation experiments were performed in October 2011, after at least 15 dry days.

S2.3. Experimental locations

The rainfall simulations were performed over the three different experimental zones described previously. A real view of each experiment is presented in Figure S3.

Figure S3 – Rainfall simulation locations:(a) waste-pile, (b) river-bed and (c) the sedimentation pond.

S3. Isolation of colloid-suspensions from runoff

S3.1. Experimental procedure

In order to separate the colloid-suspensión (CS, ≤ 1000 nm), soild colloids (1000-10 nm and the dissolved fraction (DF, < 10 nm), runoff samples were subjected to the protocol described in the Figure S4. These samples were gently shaken and homogenized before four 40 mL aliquots were transferred into four acid-cleaned polypropylene vessels and

subsequently centrifuged at 800 rpm during 10 minutes. According to the equations for size-based separation (Bolea et al., 2010), the resulting supernatants (~20 mL) corresponded to their CS. These CS were pipeted to the polypropylene vessels and stored at 4ºC. One CS aliquot was used for AF4-ICP-MS analyses within the following 48 hours. The second CS aliquot was ultrafiltered through ultrafiltration membranes (*Pall Filtron, Microsep Omega, 10-nm pore size*) to determine the As, Fe, Al, Cu, Zn and Pb concentrations in the dissolved fraction (DF) by ICP-MS or ICP-OES. Colloids with a size range of 1000-10 nm, deposited on the ultrafiltration membranes were stored at 4ºC. The colloids from the waste-pile zone (WP) were analyzed by As and Fe K-edge EXAFS and the colloids from sedimentation-pond zone (SP) by XANES spectroscopy. The third CS aliquot was used to quantify the mass of colloids contained, as described by Plathe et al. (2010) but modified as follows: 10 mL of the CS were placed onto pre-weighted glass vessels along with 6 mg of NaCl (*'suprapure', Merck*). The mixtures were shaken for 30 minutes and centrifuged at 4000 rpm for 15 min. The resulting supernatant was discarded and the colloidal mass, coagulated by the effect of the NaCl, were dried at 60°C during 24 hours, and finally weighted.

Lastly, ten milliliters of the four CS aliquot were dissolved in two digestion microwave-assisted steps by a microwave program at 200ºC during 15 min (Ethos Series 1, *Milestone*): Step I – 11.5 mL of HF/HNO_3/HCl (volume ratio 1.5:0.75:3.5) and Step II – 9 mL of H_3BO_3 (5 %). Solutions from the digestion process were filtered and measured by ICP-OES (Iris & Intrepid Radial, *Thermo Fisher Scientific*) for Fe, Al, Cu, Zn and Pb; and by ICP-MS (ELAN DRC-e, *Perkin Elmer*) for As quantification.

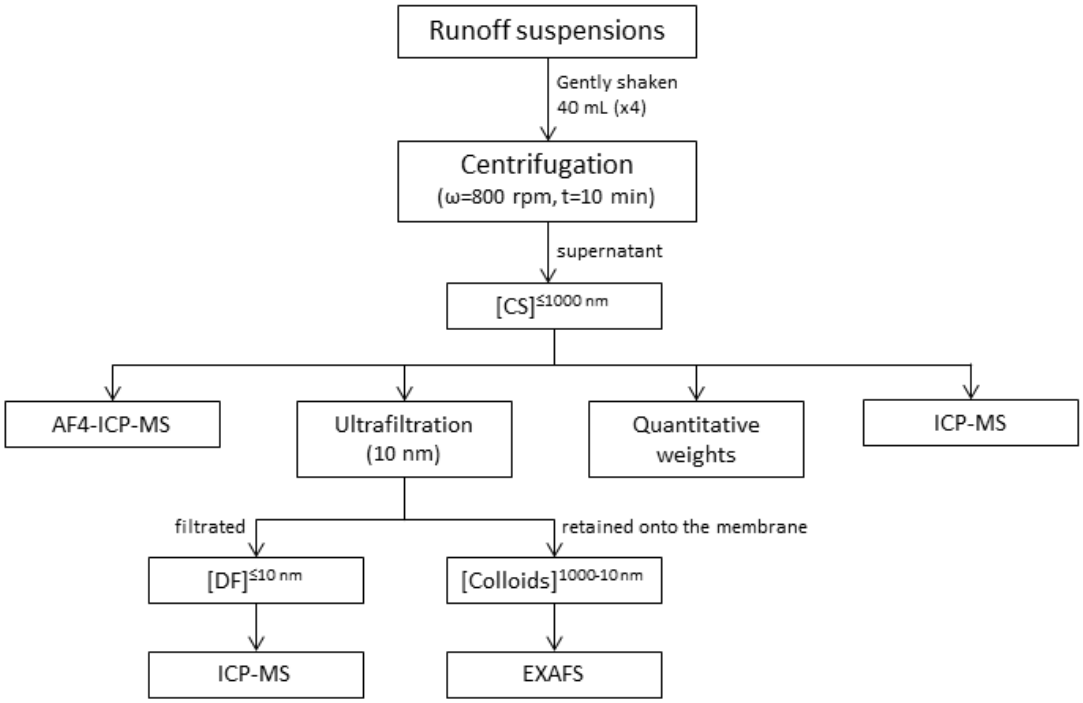

Figure S4 – Procedure for isolation and characterization of colloid-suspensions (CS, ≤ 1000 nm) from original runoff suspensions. Colloids (1000-10 nm) were isolated using ultrafiltration membranes (10 nm) and the dissolved fraction (DF < 10 nm) was subsequently measured by ICP-MS

S3.2. Runoff volumes and colloid concentration

All runoff suspensions were collected and weighted. The volumes of runoff suspensions collected during the rainfall simulations (Table 1) and the colloid concentration of the corresponding colloid suspensions (Table 2) are shown in Figure S5.

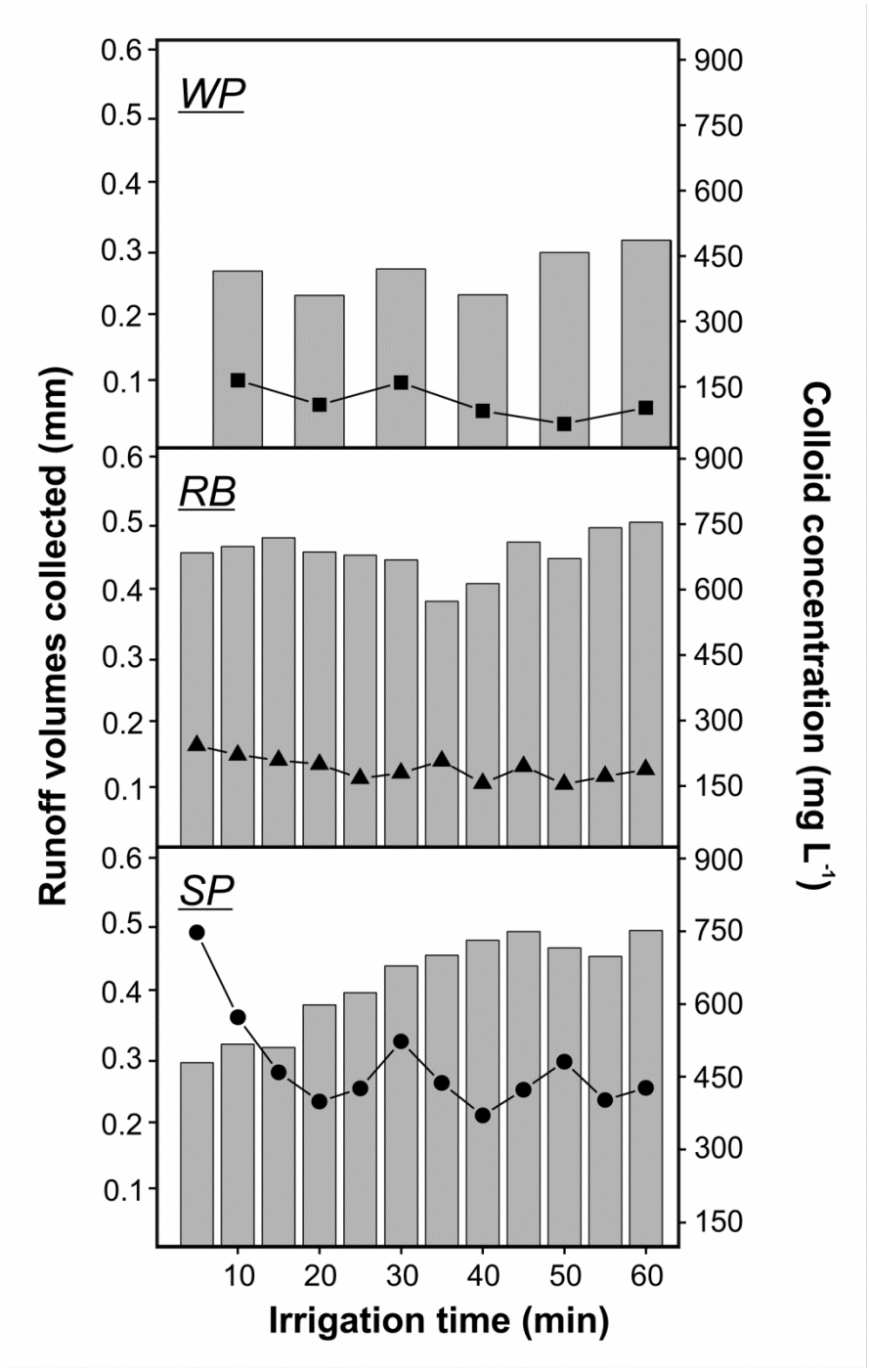

Figure S5 – Runoff volumes collected (bars, left axis) and colloidal concentration of colloid suspensions (lines and markers, right axis) at waste-pile (WP), river-bed (RB) and sedimentation-pond (SP).

S4. ICP-OES and ICP-MS analyses

The pseudo-total concentration of the samples was measured by ICP-OES after aqua regia + microwave digestion (Chen and Ma, 2001). All the chemicals used for sample preservation, analysis and reagent preparation were of analytical quality or higher. Deionized water (18 MΩ cm^{-1}, MilliQ +, *Millipore Corp.*) was used for all solutions and dilutions. Arsenic determinations were performed by ICP-MS (ELAN DRC-e, *Perkin Elmer*) while Fe, Al, Cu, Zn and Pb quantification were done by ICP-OES (Iris & Intrepid Radial, *Thermo Fisher Scientific*). For ICP analyses, calibration curves were run before and after each sample series (20 samples including matrix-matched blanks and in-between calibration checks). The calibration solutions covered the range of concentration in the samples and were prepared in the same matrix as the extracting reagents from certified stock solutions. Sample blanks were analyzed for correction of background effect on instrument response. Trace metal standards were used to assess instrument precision. We calculated metal concentrations in unknown solutions on the basis of the external calibration averaging the concentrations from two repetitions for each experimental replication. Limits of detection were calculated at three standard deviation of the instrument response from 10 repeated analyses of sample matrix-matched blank solutions. Results from ICP-OES and ICP-MS analyses are presented in Tables 3 and S1.

The companion metal concentrations to As and Fe are listed in Table S2. The aluminium concentrations in the colloid suspension and in the dissolved fraction followed a different trend than Fe. At the waste-pile zone, Al concentration was low, averaging 225 µg L^{-1} in the colloid suspension and below the quantification limit (QL) in the dissolved fraction at all sampling times. Instead, at the river-bed zone, Al concentrations were higher than those of Fe and decreased with irrigation time from

1900 µg L^{-1} to 624 µg L^{-1} and 1320 µg L^{-1} to 456 µg L^{-1} in the colloid suspension and in the dissolved fraction, respectively. In the sedimentation-pond zone, Al content in the dissolved fraction was below the QL and that in the colloid suspension increased with irrigation time from 1030 to 1700 µg L^{-1} unlike the Fe one. Copper, Zn and Pb concentrations showed different distribution patterns with the irrigation time at each sampling zone. Essentially, the importance of colloidal versus dissolved mobilization decreases in the order Pb (~100%) > Cu (~60%) > Zn (~0%) at the waste-pile zone.

Table S1 – Companion metal concentrations of selected colloid (≤ 1000 nm) suspensions (CS) and dissolved fractions (DF) ≤ 10 nm (± standard deviation, *n=3* [a])

Sample	Time	Fraction	Al	Cu	Zn	Pb
			µg L^{-1} [b,c]			
WP	20 min	*CS*	223±92	116±31	854±50	68±41
		DF	< QL	74±47	922±64	< QL
		Colloids	223 [d]	42	-	68
WP	40 min	*CS*	255±90	115±48	523±48	75±38
		DF	< QL	70±39	555±59	< QL
		Colloids	255	45	-	75
WP	50 min	*CS*	198±114	107±51	362±55	63±33
		DF	< QL	70±42	372±69	< QL
		Colloids	198	37	-	63
RB	20 min	*CS*	1900±105	1760±34	1340±57	< Q
		DF	1320±97	2040±46	1460±67	< QL
		Colloids	580	-	-	< QL
RB	35 min	*CS*	1470±97	996±46	745±50	< QL
		DF	567±83	1040±38	766±63	< QL
		Colloids	903	-	-	< QL
RB	50 min	*CS*	624±108	817±40	840±46	< QL
		DF	456±102	858±55	757±60	< QL
		Colloids	168	-	-	< QL
SP	20 min	*CS*	1030±103	63±52	317±61	< QL
		DF	< QL	< QL	65±62	< QL
		Colloids	1030	63	252	< QL
SP	35 min	*CS*	1260±86	44±39	155±54	< QL
		DF	< QL	< QL	102±66	< QL
		Colloids	1260	44	53	< QL
SP	50 min	*CS*	1700±124	20±46	114±58	< QL
		DF	< QL	< QL	63±61	< QL
		Colloids	1700	20	51	< QL

[a] *Standard deviation was calculated by triplicate determination of the same aliquot*
[b] *Elemental concentration was expressed on ng of metal per liter of colloid suspension (CS)*
[c] *Quantification limits (QL) for ICP-OES measurements were: Al = 100 µg L^{-1}, Cu = 12 µg L^{-1}, Zn = 23 µg L^{-1}, Pb = 31 µg L^{-1}*
[d] *Metal concentrations of colloids (1000-10 nm) were defined as the difference between the concentration of the CS and the DF*

S5. Asymmetric flow field-flow fractionation

S5.1. AF4 characteristics

The channel dimensions were 27.5 cm in length and from 2 to 0.5 cm in width. The spacer used for all the measurements had 350 μm thickness. The accumulation wall consisted of a 1 kDa polyethersulfone (PES) (*Postnova Analytics*). Novachem surfactant (*0.01 %, w/v, Postnova Anlytics*) adjusted to pH = 4.5 was used as carrier solution. Carrier was degased prior to use by an on-line vacuum degasser. The out flow was 0.8 mL min^{-1} and a sample loop of 100 μL was used throughout. Colloid-suspensions and calibration standards were detected using a UV-vis diode array detector (*Shimadzu*, wavelength range: 200 to 650 nm). The AF4-UV-vis system was coupled to an ICP-MS in order to perform an on-line multi-element quantification. Samples were introduced into the ICP-MS using a glass concentric slurry nebulizer and a cyclonic spray chamber (*Glass Expansion*). An internal standard solution of 50 ng mL^{-1} Rhodium (*Merck*) was merged with the carrier at 0.3 mL min^{-1} for correction of instrumental drift. The instrumental conditions of the AF4-ICP-MS system are presented in Table S2.

Table S2 – AF4 operating conditions and ICP-MS instrumental and data acquisition parameters

Crossflow program of AF4			
Carrier	*Time (min)*	*Crossflow type*	*Crossflow (mL min^{-1})*
Novachem 0.01%, pH = 4.5 [a]	35	Constant	0.1
	3	Linear Decay	0
	2	Constant	0
Instrumental parameters of ICP-MS			
RF power		1200 W	
Argon gas flow rate			
Plasma		15 L min^{-1}	
Auxiliary		1.2 L min^{-1}	
Nebulizer		0.9 L min^{-1}	
Data acquisition parameters of ICP-MS			
Measuring mode		Peak hoping	
Points per spectral peak		1	
Dead time		60 ns	
Sweeps		10	
Dwell time		5 ms	
Integration time per point		50 ms	
Settle time		3 ms	

[a] *Outflow = 0.8 mL min^{-1}*

S5.2. AF4 principles and channel calibration

According to the AF4 theory, in normal mode it is possible to establish a relationship between a retention parameter (λ) and the diffusion coefficient (D) of the eluted specie, which can be related to their hydrodynamic diameter (d) using the Stokes-Einstein equation (Assemi et al., 2004).

Since the colloid-suspension (CS) have a size lower than 1000 nm, the AF4 will be operated only in normal mode, and the relationship between the retention ratio and size could be obtained using a set of size standards (Schimpf et al., 2000), assuming a similar behavior between the size standards and the particles to be characterized. Monodispersed size standards of silicon dioxide [SiO_2] of 0.020 ± 0.004, 0.15 ± 0.03 and 0.50 ± 0.05 µm were used for AF4 calibration. These standards were used because of its similar nature to the colloid samples. The calibration curve obtained for normal mode was: log R = -2.066 – 0.934 log d (r = 0.991), where d is the particle diameter in µm, and R = t_0/t_r, where t_0 is the elution time corresponding to the void peak and t_r is the

retention time for a given particle. Diluted solutions (20 mg L^{-1}) of these standards (*Sigma-Aldrich*) were prepared by further dilution with the corresponding carrier.

S5.3. AF4-ICP-MS measurements

Within the following 48 hours after performing the rainfall simulation tests, all the colloid (≤ 1000 nm) suspensions were isolated and measured by AF4-ICP-MS. The colloid suspensions from the waste-pile and the river-bed could not be measured by AF4, as presented in the Figure S6.

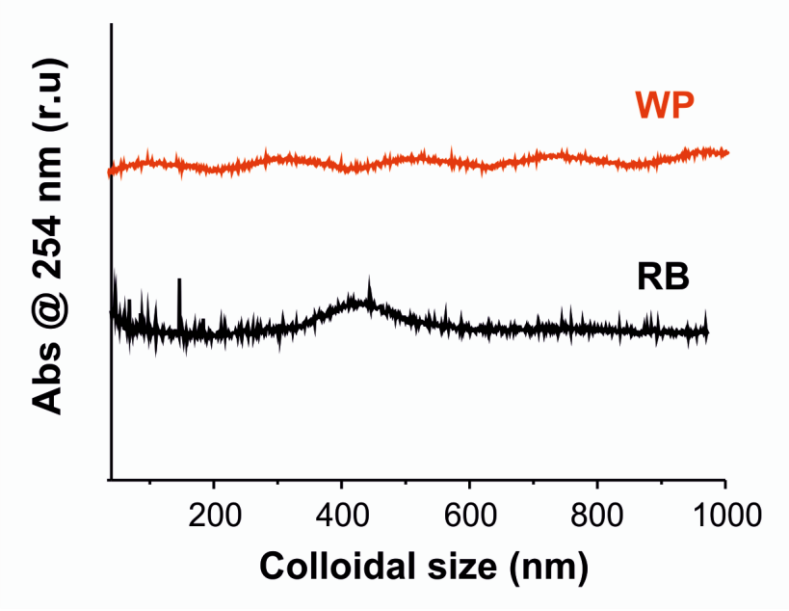

Figure S6 – AF4 fractograms of colloid suspensions from waste-pile (WP) and river-bed (RB) at 20 minutes

The particle size distribution and associated As, Fe and Al concentrations of colloid suspensions at 20, 35 and 50 minutes in sedimentation-pond zone were calculated by AF4-ICP-MS (Figure S7). The maxima concentration peaks were identified by fitting a lognormal function and calculating the maximum and confidence interval at 95 % probability (Figure 1b).

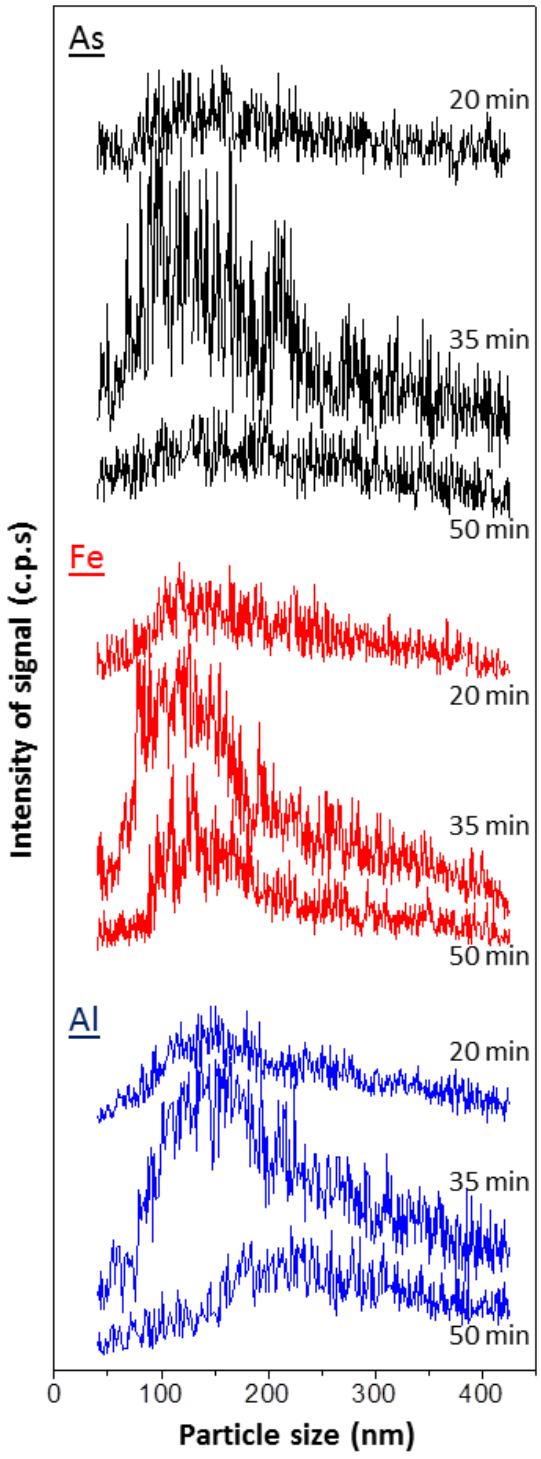

Figure S7 – Arsenic, iron and aluminum AF4-ICP-MS bulk fractograms of the colloid suspensions from sedimentation-pond collected at 20 minutes, 35 minutes and 50 minutes.

S4.4. Recovery calculations

The recovery of the AF4 determination is a parameter which provides additional information. Reference calculations were made using three injections of sample without applying any crossflow in the AF4 channel (no injection step was applied either). Then, three injections were performed applying the crossflow program described in Table S3. Afterwards, peaks areas were calculated from signal and the recoveries expressed as: $R\ (\%) = S/S_0 \cdot 100$, where S is the signal area obtained when a crossflow is applied, and S_0 is the signal area obtained with no crossflow. The AF4-ICP-MS recoveries of the colloid suspensions from sedimentation-pond are presented in Table S3.

Table S3 – Recoveries of colloid suspensions from sedimentation-pond (SP) and target metals obtained by AF4-ICP-MS measurements [a]

DCF	**Irrigation time**	**AF4-ICP-MS recovery (%)**		
		As	***Fe***	***Al***
SP	*20 min*	23	48	58
	35 min	25	65	51
	50 min	17	48	39

[a] *Three AF4 injections were averaged to calculate the recoveries shown*

Taking into account that approximately three quarters of total As found in the sedimentation-pond are presented in the dissolved fraction (DF ≤ 10 nm), arsenic recoveries ranging 17-25 % are in agreement with the As presented in the colloid-suspension (Table 3). Iron and Al recoveries are comparable to those found in similar studies by AF4-ICP-MS (Serrano et al., 2015), as reported by Neubauer et al. (2013) who explained that lower recoveries than expected are generally associated with adsorption processes of the species injected onto the permeation membrane of the channel, or with losses by filtration through the membrane of those species with molecular weight lower than its pore size (< 1 kDa).

S6. X-ray absorption spectroscopy

S6.1. Data analysis

The colloid-bearing ultrafiltration membranes were placed on holders made of polyether ether ketone (PEEK) material and sealed with Kapton® tape. Arsenic and Fe K-edge EXAFS spectra were recorded at the bending magnet BM25A beamline at the European Synchrotron Radiation Facility (ESRF, Grenoble, France) (6 GeV, 100 mA, Si(111) monochromator crystals) at room temperature (RT) using a 13-element Ge(Li) solid state detector. Additional As EXAFS spectra from the SP colloids were recorded at beamline 22 of the ALBA Synchrotron Facility (Barcelona, Spain) (3 GeV, 400 mA, Si(311) monochromator) at 80°K using a CdTe solid state detector. The beam energy was calibrated by setting the first inflection point in the K absorption edge of a metallic Fe foil to 7112 eV (Fe measurements) or the first maximum in the K absorption edge of KH_2AsO_4 (*Sigma-Aldrich*) to 11875 eV (As measurements). The sample spectra were acquired in fluorescence mode, starting at 6950 eV (Fe) or 11650 eV (As). The pre-edge step size was set to 5 eV, and the edge step size along the edge was set to 0.5 eV. The EXAFS spectra were collected up to 9 $Å^{-1}$ for Fe and 10.5 $Å^{-1}$ for As respectively, using a step size of 0.05 $Å^{-1}$ in k-space with constant measurement times over the entire EXAFS range. The sample spectra were obtained by averaging several replicate scans (10-12 scans at ESRF; 3-4 at ALBA).

Arsenic and iron normalized K-edge XANES spectra were initially compared with the reference compounds and presented in Figure S8 together with their first derivatives.

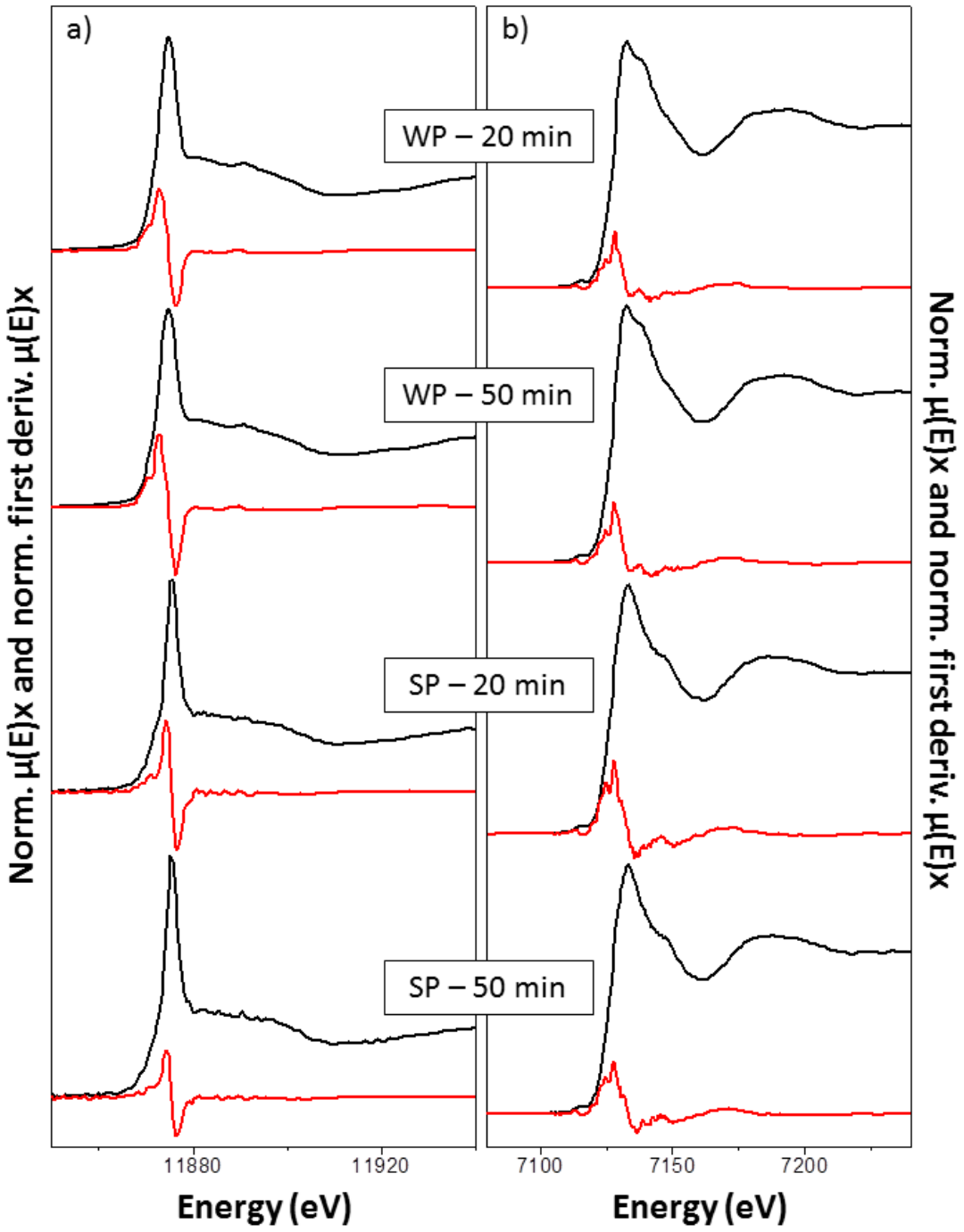

320

321 Figure S8 – Normalized As (a) and Fe (b) K-edge XANES spectra (black line) and their

322 first derivatives (red line) of colloids (1000-10 nm) from waste-pile (WP) and

323 sedimentation-pond (SP) at 20 minutes and 50 minutes of runoff.

324

325

Firstly, the entire library (sixteen spectra for Fe, twelve spectra for As) was screened to determine combinations of reference spectra that best matched the data. Subsequently, the k^3-wheighted EXAFS spectra of waste-pile (WP) colloids were analyzed by linear least-squares combination fittings (LCF) over the k-range 2-8 $Å^{-1}$ for Fe and 2-11 $Å^{-1}$ for As, while the XANES spectra of sedimentation-pond (SP) colloids were also analyzed by LCF over the range – 30 eV and + 60 eV for both As and Fe (Table 4). On the basis of their occurrence and relevance in those preliminary fits, the following reference spectra were included in the final fits which allowed to reproduce all sample EXAFS spectra: An arsenate (scorodite) and As(V) sorbed onto Fe(III)-(hydr)oxides (ferrihydrite) were selected for As LCF analyses; while we used different Fe(III)-(hydr)oxides (e.g., scorodite, ferryhidrite, hematite), different Fe-bearing phylosillicates (e.g., smectite, nontronite) and a Fe(III)-(oxy)sulfides (schwertmannite) in the Fe fittings.

Reference and sample spectra were processed and analyzed by linear combination fitting (LCF) using the software code Athena (Ravel and Newville, 2005). The E_0 was fixed at 7128.5 eV for Fe and 11875 eV for As. The background was substracted using a linear fit through the pre-edge region and the Autobk routine in Athena for the spline fit through the EXAFS region (R_{bkg} = 0.8 for As and 0.9 for Fe, *k*-weight = 3, spline *k*-range = 0.5 – 10.5 $Å^{-1}$ for As and 0.5 – 8.5 $Å^{-1}$ for Fe).

In the case of As, starting from the best fit with one component, the number of components *n* was increased as long as the normalized sum of the squared residuals ($NSSR = \sum(data_i - fit_i)^2/\sum(data_i)^2$) of best *n* + 1-component fit was at least 10% lower than the NSSR of the best *n*-component fit. Otherwise, in the Fe LCF, the best *n* + 1-component fit was considered to be significantly better than the best *n*-component fit, if its NSSR was at least 20% lower and if no component account for less than 5% of total

Fe. Linear combination fittings were not constrained to sum 100% (Table 3). More details of reference compound spectra, including their synthesis as well as the reference publications, are shown in Table S4.

Table S4 – As and Fe reference compounds used for linear combination fitting

As standards				
Name	**Group**	**Type**	**Beamline**	**Source**
Scorodite	Arsenate	Natural	BM 4-3, SSRL	Savage et al. (2005)
As(V) sorbed to ferrihydrite	Fe(III) oxide	Synthetic	BM 4-3, SSRL	Root et al. (2009)
Fe standards				
Name	**Group**	**Type**	**Beamline**	**Source**
Scorodite	Oxide	Natural	BM 4-3, SSRL	Savage et al. (2005)
Ferrihydrite	Oxide	Synthetic	XAS BM, ANKA	Voegelin et al. (2010)
Hematite	Oxide	Natural	BM 7-3, SSRL	O'Day et al. (2004)
Schwertmannite	Oxy-sulfate	Synthetic	BM 4-1, SSRL	measured by S. Hayes [a]
Smectite	Phyllosilicate	Natural	BM 2-3, SSRL	O'Day et al. (2004)
Nontronite	Phyllosilicate	Natural	XAS BM, ANKA	Gorski et al. (2013)

[a] *Unpublished reference EXAFS spectrum*

S6.2 Shell-fittings

Least-squares fitting of k^3-weighted Fe and As K-edge spectra were then performed in Artemis (Ravel and Newville, 2005), only for the waste-pile colloids collected at 20 and 50 minutes (Table S5). Theoretical single and multiple scattering paths used to model both the Fe and the As K-edge EXAFS spectra were calculated from the structure of scorodite (Kitahama et al., 1975), using FEFF 8.2 (Ankudinov and Rehr, 2000).

The As K-edge EXAFS spectra were fitted in *R*-space over a distance $R + \Delta R$ of 0.8 – 3.6 Å (k-weigh = 3, Kaiser-Bessel window sill = 2 $Å^{-1}$). Two single scattering (SS) paths were used to model the spectra: As-O and As-Fe. Multiple scattering (MS) within AsO_4 tetrahedra was accounted for by a three-legged triangular As–O–O MS path (degeneracy = 12). According to Mikutta et al. (2013), the addition of four-legged MS paths involving As and O atoms were of minor importance to model the As K-edge EXAFS of scorodite. In addition, the low data quality of collected EXAFS spectra

supported the use of only the triangular As–O–O MS path. While the degeneracies of the MS path were fixed to their theoretical value, their half path lengths were expressed as a function of the SS As–O half path length assuming an ideal tetrahedron. The half path length of the triangular As–O–O MS path were set to 1.8165 (=1 + $\sqrt{(2/3)}$) times the As–O SS half path length. The Debye-Waller parameters for the MS paths were constrained by considering the correlation between the lengths of individual legs (Hudson et al., 1996). Assuming that the lengths of the As–O and the O–As leg of the triangular As–O–O MS path are not correlated, their contribution to the σ^2 of MS half path length equals half the σ^2 of As–O SS path. However, because also the O–O leg contributes to the σ^2 of the MS path, we assumed the σ^2 of the MS path to be equal to the σ^2 of the As–O SS path (Voegelin et al., 2007).

The k^3-weighted Fe K-edge EXAFS spectra were Fourier-transformed over the k-range 2.5 – 10.5 Å^{-1} using a Kaiser-Bessel window (sill width = 2.5 Å^{-1}). The fits were performed in *R*-space over a distance $R + \Delta R$ of 0.9 – 3.8 Å. Shell fits include two SS paths for the first and second coordination shells of Fe (Fe –O, Fe–As). In addition, one MS within FeO_6 octahedra was accounted for: a triangular Fe–O–O MS path (degeneracy = 24, $\sigma^2 = \sigma^2$ (Fe–O SS)). The half path length of the triangular Fe–O–O MS path were set to 1.7071 (=1 +$\frac{\sqrt{2}}{2}$) times the Fe–O SS half path length (Voegelin et al., 2010).

Table S5 – Shell-fit results for As and Fe K-edge EXAFS spectra of colloids (1000-10 nm) isolated from colloid suspensions sampled after 20 and 50 minutes of rainfall in waste-pile (WP) zone. Theoretical simple and multiple scattering paths were calculated from the structure of scorodite (Kitahama et al. 1975) using FEFF 8.2 (Ankudinov and Rehr, 2000)

As shell-fit parameters [a]

Sample	Path	N [b]	σ^2 [c] ($Å^2$)	R [d] (Å)	S_0^2 [e]	ΔE [f] (eV)	R-factor [g]	red γ^2 [h]
WP 20 min	*As-O*	**4**	0.0016	1.68	1.06	3.54	0.0405	$2.77 \cdot 10^6$
	As-Fe	**2**	0.0021	3.36				
	MS1 [i]	**12**	0.0064	3.08				
WP 50 min	*As-O*	**4**	0.0019	1.69	1.06	3.39	0.0390	$3.88 \cdot 10^6$
	As-Fe	**2**	0.0021	3.36				
	MS1 [i]	**12**	0.0077	3.08				

Fe shell-fit parameters [a]

Sample	Path	N [b]	σ^2 [c] ($Å^2$)	R [d] (Å)	S_0^2 [e]	ΔE [f] (eV)	R-factor [g]	red γ^2 [h]
WP 20 min	*Fe-O*	**6**	0.0074	1.98	1.02	- 2.57	0.0545	$3.97 \cdot 10^5$
	Fe-As	**4**	0.0074	3.35				
	MS2 [j]	**24**	0.0074	3.46				
WP 50 min	*Fe-O*	**6**	0.0079	1.98	1.02	- 2.84	0.0517	$4.24 \cdot 10^5$
	Fe-As	**4**	0.0068	3.35				
	MS2 [j]	**24**	0.0079	3.46				

[a] *The fit range was set to 2.5 - 10.5 Å*
[b] *Degeneracy (coordination number for single scattering paths), values in bold were fixed during shell fitting*
[c] *Debye-Waller parameter, uncertainty for As-O ± 0.0010-0.0016 Å², for As-Fe ± 0.0032-0.0040 Å², for Fe-O ± 0.0017-0.0022 Å²*
[d] *Half path length (inter-atomic distance for single scattering paths), uncertainty for As-O ± 0.013-0.015 Å, for As-Fe ± 0.0033-0.0037 Å, for Fe-O ± 0.013-0.016 Å*
[e] *Amplitude correction factor, constrained to the same value for all paths in a simultaneous fit*
[f] *Energy shift, constrained to the same value for all paths in a simultaneous fit, uncertainty < ± 1.2 eV*
[g] *Normalized sum of the squared residuals of the fit ($R = \sum(data-fit)^2 / \sum data^2$)*
[h] *Reduced γ^2 (Stern et al. 1995)*
[i] *MS1 = Triangular As-O-O MS path within As(V) tetrahedron, degeneracy = 12*
[j] *MS2 = Triangular Fe-O-O MS path within Fe(III) octahedron, degeneracy = 24*

S7. References

Ankudinov AL, Rehr JJ. Theory of solid-state contributions to the x-ray elastic scattering amplitude. Physical Review B 2000; 62: 2437-2445.

Assemi S, Newcombe G, Hepplewhite C, Beckett R. Characterization of natural organic matter fractions separated by ultrafiltration using flow field-flow fractionation. Water Research 2004; 38: 1467-1476.

Barnishel R, Bertsch PM. Methods of Soil Analysis. Part 2. Chemical, Microbiological Properties. Aluminum 1982; American Society of Agronomy: 275-300.

Bolea E, Laborda F, Castillo JR. Metal associations to microparticles, nanocolloids and macromolecules in compost leachates: Size characterization by asymmetrical flow field-flow fractionation coupled to ICP-MS. Analytica Chimica Acta 2010; 661: 206-214.

Calvo A, Gisbert J, Palau E, Romero M. Eds. M. Sala and F. Gallart 1988; SEG Monogr.: 6-15, Spain.

Cerda A, Ibanez S, Calvo A. Design and operation of a small and portable rainfall simulator for rugged terrain. Soil Technology 1997; 11: 163-170.

Chen M, Ma LQ. Comparison of three aqua regia digestion methods for twenty Florida soils. Soil Science Society of America Journal 2001; 65: 491-499.

Gee GW, Bauder JW. Methods of Soil Analyses. Part 1. Physical and mineralogical methods 1986; Particle-size analyses. Madison, WI.: 383-411.

Gorski CA, Klüpfel LE, Voegelin A, Sander M, Hofstetter TB. Redox Properties of Structural Fe in Clay Minerals: 3. Relationships between Smectite Redox and Structural Properties. Environmental Science & Technology 2013; 47: 13477-13485.

438 Hudson EA, Allen PG, Terminello LJ, Denecke MA, Reich T. Polarized x-ray-
439 absorption spectroscopy of the uranyl ion: Comparison of experiment and
440 theory. Physical Review B 1996; 54: 156-165.
441 Kitahama K, Kiriyama R, Baba Y. Refinement of crystal-structure of Scorodite. Acta
442 Crystallographica Section B-Structural Science 1975; 31: 322-324.
443 Mikutta C, Mandaliev PN, Kretzschmar R. New Clues to the Local Atomic Structure of
444 Short-Range Ordered Ferric Arsenate from Extended X-ray Absorption Fine
445 Structure Spectroscopy. Environmental Science & Technology 2013; 47: 3122-
446 31.
447 Neubauer E, von der Kammer FD, Hofmann T. Using FLOWFFF and HPSEC to
448 determine trace metal colloid associations in wetland runoff. Water Research
449 2013; 47: 2757-2769.
450 O'Day PA, Vlassopoulos D, Root R, Rivera N. The influence of sulfur and iron on
451 dissolved arsenic concentrations in the shallow subsurface under changing redox
452 conditions. Proceedings of the National Academy of Sciences of the United
453 States of America 2004; 101: 13703-13708.
454 Plathe KL, von der Kammer F, Hassellov M, Moore J, Murayama M, Hofmann T, et al.
455 Using FlFFF and aTEM to determine trace metal-nanoparticle associations in
456 riverbed sediment. Environmental Chemistry 2010; 7: 82-93.
457 Ravel B, Newville M. Athena and Artemis: interactive graphical data analysis using
458 IFEFFIT. Physica Scripta. 2005; T115: 1007–1010.
459 Root RA, Vlassopoulos D, Rivera NA, Rafferty MT, Andrews C, O'Day PA. Speciation
460 and natural attenuation of arsenic and iron in a tidally influenced shallow
461 aquifer. Geochimica Et Cosmochimica Acta 2009; 73: 5528-5553.

462 Savage KS, Bird DK, O'Day PA. Arsenic speciation in synthetic jarosite. Chemical
463 Geology 2005; 215: 473-498.
464 Schimpf ME, Caldwell K, Giddings JC. Field-Flow Fractionation Handbook. In: Wiley
465 & Sons (ed) 2000.
466 Serrano S, Gomez-Gonzalez MA, O'Day PA, Laborda F, Bolea E, Garrido F. Arsenic
467 speciation in the dispersible colloidal fraction of soils from a mine-impacted
468 creek. Journal of Hazardous Materials 2015; 286: 30-40.
469 Shuman LM. Fractionation method for soil microelements. Soil Science 1985; 140: 11-
470 22.
471 Thomas GW. Methods of Soil Analysis, Part 2. Chemical and Microbiological
472 Properties. Exchangeable cations 1982; Soil Science Society of America: 159-
473 166.
474 Voegelin A, Kaegi R, Frommer J, Vantelon D, Hug SJ. Effect of phosphate, silicate,
475 and Ca on Fe(III)-precipitates formed in aerated Fe(II)- and As(III)-containing
476 water studied by X-ray absorption spectroscopy. Geochimica Et Cosmochimica
477 Acta 2010; 74: 164-186.
478 Voegelin A, Weber FA, Kretzschmar R. Distribution and speciation of arsenic around
479 roots in a contaminated riparian floodplain soil: Micro-XRF element mapping
480 and EXAFS spectroscopy. Geochimica Et Cosmochimica Acta 2007; 71: 5804-
481 5820.
482 Walkley A, Black IA. An examination of the Degtjareff method for determining soil
483 organic matter, and a proposed modification of the chromic acid titration
484 method. Soil Science 1934; 37: 29-38.

485